Journal of Applied Polymer Science

# Effects of processing parameters and thermal history on microcellular foaming behaviors of PEEK using supercritical $CO_2$

**Quan Yang, Guangcheng Zhang, Zhonglei Ma, Jiantong Li, Xiaolong Fan**
Department of Applied Chemistry, School of Science, Northwestern Polytechnical University, Xi'an 710072, China
Correspondence to: G. Zhang (E-mail: zhangguc@nwpu.edu.cn)

**ABSTRACT:** In this study, we mainly investigate the solid-state foaming of polyether ether ketone (PEEK) with different crystallinities using supercritical $CO_2$ as a physical blowing agent. The gaseous mass-transfer and thermophysical behaviors were studied. By altering the parameters of the foaming process, microcellular foams with different cell morphologies were prepared. The effect of crystallization on the cell morphology was also investigated in detail. The results indicate that the crystallization restricts gas diffusion in the material, and the thermophysical behaviors of the saturated PEEK sample with low crystallinity presents two cold crystallization peaks. The cell density decreases and the cell size increases as the saturation pressure increases. The cell density of the microcellular foams prepared under 20 MPa is $1.23 \times 10^{10}$ cells/cm$^3$, which is almost 10 times compares to that under 8 MPa. The cell size increases as the foaming time extends or the foaming temperature increases. It is interesting that the cell morphology with a bimodal cell-size distribution is generated when the samples are foamed at temperatures higher than 320°C for a sufficient time. Additionally, nanocellular foams can be obtained from a highly crystallized PEEK after the decrystallization process. © 2015 Wiley Periodicals, Inc. J. Appl. Polym. Sci. **2015**, *132*, 42576.

**KEYWORDS:** crystallization; differential scanning calorimetry; foams; microscopy; properties and characterization

Received 13 December 2014; accepted 4 June 2015
**DOI: 10.1002/app.42576**

## INTRODUCTION

Microcellular foam is a new type of cellular material having a cell density larger than $10^9$ cells/cm$^3$, and an average cell size of around 10 $\mu$m, which is much smaller than that of the conventional foam.[1] The production of microcellular foams using carbon dioxide ($CO_2$) or nitrogen ($N_2$) as a physical blowing agent was first described by Martini in the early 1980s.[2] A microcellular structure of thermoplastic polymers can be developed by the solid-state foaming process: a polymer sample was first saturated under high-pressure gas for sufficient time, and followed by a process of either rapidly decreasing pressure or increasing temperature. Compared with solid polymer, microcellular foam offers multiple advantages, including a significant reduction in material cost and weight, elevated toughness and energy absorption, good sound and thermal insulation, improved fatigue life, and decreased electrical constant.[3–9] Due to these superior properties, microcellular foam has been widely used as lightweight structural materials in applications such as aerospace, automotive, thermal and electrical insulation, packaging, etc.[10,11]

With the development of supercritical fluid foaming technology, novel microcellular foams with high-temperature resistance, corrosion resistance, and mechanical strength are developed constantly to meet the need in the harsh environment areas.[12–14] In the field of microelectronics, for example, foams require a certain degree of heat resistance to inhibit deformation of cells.[15] Therefore, the development of high-performance foams has become an important research direction.[13]

Microcellular foaming of the semicrystalline polymer using supercritical $CO_2$ is a hotspot as the semicrystalline microcellular foam has a higher strength and stiffness, as well as a smaller cell structure compared with the amorphous microcellular foam.[16] However, it is relatively difficult to control cell structure of the semicrystalline polymers compared with that of the amorphous ones. The structurally heterogeneous nature of the semicrystalline polymers has a large impact on the gas dispersion in the polymer matrix, which affects the cell nucleation and growth during foaming process. Doroudiani *et al.*[17] observed a uniform cell morphology generated in a low-crystallinity polymer, while a nonuniform structure formed in a high-crystallinity polymer. They explained that polymers with different crystallinities show different gas solubility. Itoh *et al.*[18] observed that cell nucleation was induced in the surroundings of crystalline regions, when the foaming temperature of polyphenylene sulfide was above its crystallization temperature.

Nanocellular foam refers to a novel cellular material having a cell size in the range of nanometers.[19] Studies of nanocellular

**Table I.** Characteristic Temperatures, Enthalpy Values, and Crystallinities Calculated from DSC Thermograms

| Sample # | $T_g$ (°C) | $T_{cc}$ (°C) | $T_m$ (°C) | $\Delta H_{cc}$ (J/g) | $\Delta H_m$ (J/g) | $X_c$ (%) | $CO_2$ concentration (%) |
|---|---|---|---|---|---|---|---|
| A | 141 | 176 | 339 | 20.3 | 33.2 | 10.0 | 5.9 |
| B | 157 | — | 339 | — | 35.3 | 27.2 | 2.3 |
| A′ | 153 | — | 335/350 | — | 29.1 | 22.4 | 2.6 |
| B′ | 145 | 169 | 329/347/354 | 7.9 | 32.0 | 18.5 | 3.3 |

foam are well concerned since it has been expected that nanocellular foam offers many properties such as an improved strength, toughness, and thermal insulation.[20] In addition, a small cell size makes it possible to use as some thin foam devices.[21] However, the processing techniques available to produce nanocellular foam are quite limited, and seldom have studies reported on mechanical or thermal properties of nanocellular foams.[20] Dustin *et al.*[22] produced a nanocellular structure in PEI sample when the saturation pressure is raised to 5 MPa. The nanocellular structure was produced with a cell size between 30 and 120 nm and cell density on the order of $10^{14}$ cells/cm$^3$. Krause *et al.*[23] reported that above a critical threshold of the $CO_2$ concentration, the cell morphology of homogeneous polysulfone/polyimide blend changed from microcellular into open nanocellular.

The main research of the high-performance foam focuses on amorphous polyether sulfone and polyether imide, etc. Polyether ether ketone (PEEK), as a semicrystalline polymer and special engineering plastic, presents a favorable combination of mechanical property, chemical resistance, high-temperature resistance, and radiation resistance.[24,25] Therefore, in this work, PEEK was chosen to conduct a solid-state microcellular foaming process. The gas sorption and desorption behaviors in PEEK samples with two different crystallinities were investigated firstly. The foaming behavior and thermophysical behavior of a low-crystallinity PEEK sample was investigated in detail. The effect of crystal distribution on the cell morphology as a key point was discussed in the last part of this article.

## EXPERIMENTAL

### Materials

The PEEK pellets (021G, the density of 1.32 g/cm$^3$) used in this study was purchased from Changchun Jilin University Special Plastic Engineering Research Co., Ltd. The glass transition temperature and melting temperature given by the company information are 143 and 334°C, respectively, and the dielectric constant of PEEK pellets is 3.4. PEEK pellets were first seasoned in the oven of 100°C for 4 h, and then melt-extruded into sheets (thickness of 1.2 mm) using a HAAKE Torque Rheometer–single-screw extruder (Thermo Fisher Scientific Inc. USA) at 380°C. PEEK sheets with two different crystallinities, noted as A and B, were obtained by quenching in the water and free-cooling in the air, respectively. DSC measurements revealed that the crystallinity of samples A and B were 10.0% and

**Table II.** Henry's Law Constants Calculated from Adsorption Curves

| Sample # | $k_D$ (MPa$^{-1}$) |
|---|---|
| A | 0.1589 |
| B | 0.0545 |

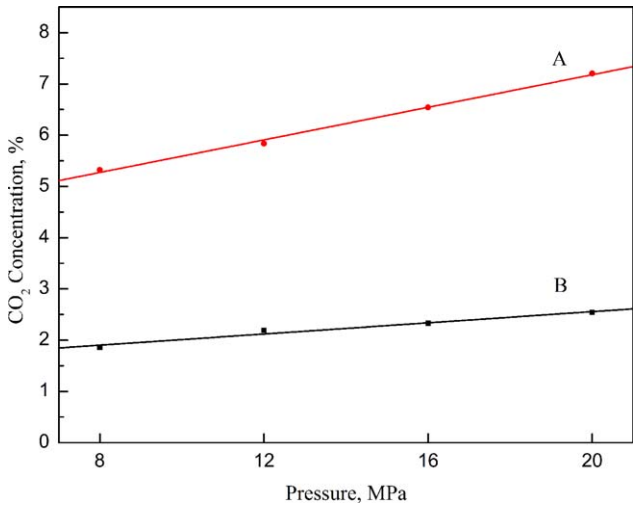


**Figure 1.** Plots of $CO_2$ concentration as a function of pressure (sample were saturated at 8–20 MPa and 45°C for 9 h). [Color figure can be viewed in the online issue, which is available at wileyonlinelibrary.com.]

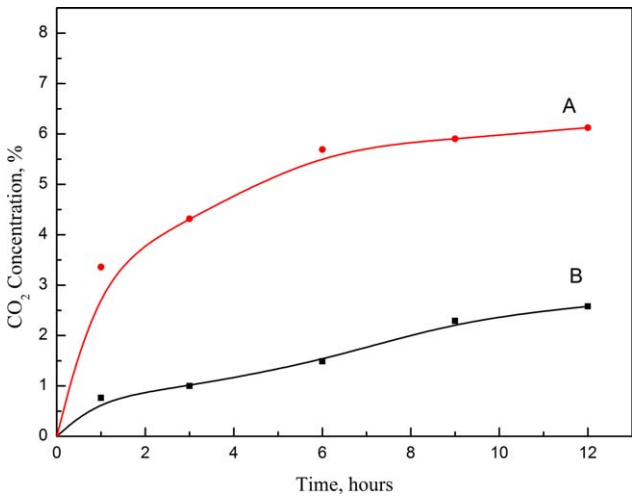


**Figure 2.** Plots of $CO_2$ concentration as a function of time (sample were saturated at 12 MPa and 45°C). [Color figure can be viewed in the online issue, which is available at wileyonlinelibrary.com.]

27.2%, respectively, as listed in Table I. The sheets were then cut into 3 × 6 cm specimens with a cutter for sorption, desorption, and foaming studies. Carbon dioxide (purity 99.99%) was purchased from Changte Airproduct Co., Xian, China.

**Gas Saturation and Desorption**

The absorption of $CO_2$ in PEEK samples were carried out in a high-pressure vessel that controlled accurately by a delicate temperature controller. The known weight of PEEK samples were first put into the high-pressure vessel, and the low-pressure $CO_2$ was delivered into the high-pressure vessel from the gas tank for about 2 min to exclude the impurities inside. Subsequently, the high-pressure $CO_2$ was delivered into the high-pressure vessel to reach a predetermined pressure (8–20 MPa) using a supercritical fluid pump (SSI, S10SNXP1) at a moderate temperature of 45°C. After absorbed for a period time (1–12 h), PEEK samples were quickly taken out from the high-pressure vessel, and weighed. Sorption of $CO_2$ on PEEK was calculated by

$$w = \frac{M_s - M_0}{M_0} \times 100\% \quad (1)$$

Where $w$ is the $CO_2$ concentration and $M_0$ and $M_s$ are the weight of the untreated and saturated PEEK samples, respectively. In desorption experiments, fully saturated PEEK samples were removed from the high-pressure vessel, and desorbed at room temperature and atmospheric pressure.

**Foaming Procedure**

PEEK samples were first saturated at a predetermined pressure and a moderate temperature of 45°C for 9 h. Subsequently, the $CO_2$ was rapidly released by turning on the valve of the high-pressure vessel within 30 s to induce cell nucleation. Then the saturated samples were quickly taken out and foamed in the silicon oil bath maintained at a predetermined temperature (240–340°C). After foaming for a period of time, the samples were immediately taken out from the silicon oil bath, and cleaned with ethanol to remove the residual silicon oil on the surface of the samples. Eventually, microcellular PEEK samples were obtained.

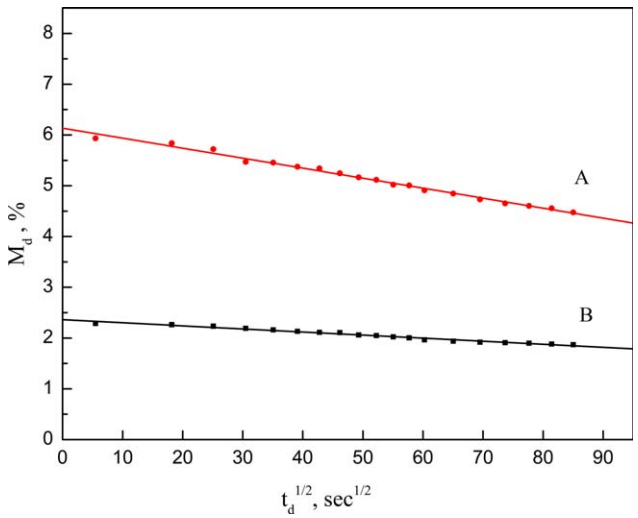


**Figure 3.** Plots of gas concentration as a function of the square root of desorption time (samples were saturated at 12 MPa and 45°C for 9 h). [Color figure can be viewed in the online issue, which is available at wileyonlinelibrary.com.]

**Table III.** $M_\infty$ and $D_d$ Calculated from Desorption Curves in Figure 3

| Sample # | $M_\infty$ (%) | $D_d$ ($m^2$/s) |
|---|---|---|
| A | 6.1336 | $3.53 \times 10^{-12}$ |
| B | 2.3615 | $2.25 \times 10^{-12}$ |

**Material Characterization**

The microcellular morphology of foamed PEEK samples was observed by a TESCAN (VEGA 3 LMH) scanning electron microscope (SEM). Specimens were first freeze-fractured with liquid nitrogen to expose the cross-sectional cellular structure. Samples were then sputter coated with Au for 60 s and placed into the SEM to observe the microcellular morphology of samples. The obtained SEM micrographs were analyzed using the software Image-Pro Plus.

The DSC measurements were conducted from 25 to 360°C at a rate of 10°C/min using a METTLER TOLEDO differential scanning calorimeter (DSC-1, Switzerland) under nitrogen atmosphere. The characteristic temperatures and the enthalpy values are obtained by DSC curves. The crystallinity was calculated by the following formula:[26]

$$X_c = \frac{\Delta H_m - \Delta H_{cc}}{\Delta H_m^o} \times 100\% \quad (2)$$

Where $\Delta H_m$ and $\Delta H_{cc}$ are the measured enthalpies of melting and cold crystallization during the DSC heating scan, respectively; $\Delta H_m^o$(130 J/g) is the melting enthalpy of 100% crystalline PEEK.[27]

The density of PEEK samples was measured according to ASTM D792, using the Archimedes water displacement technique, in which samples were weighed in air and water, respectively.

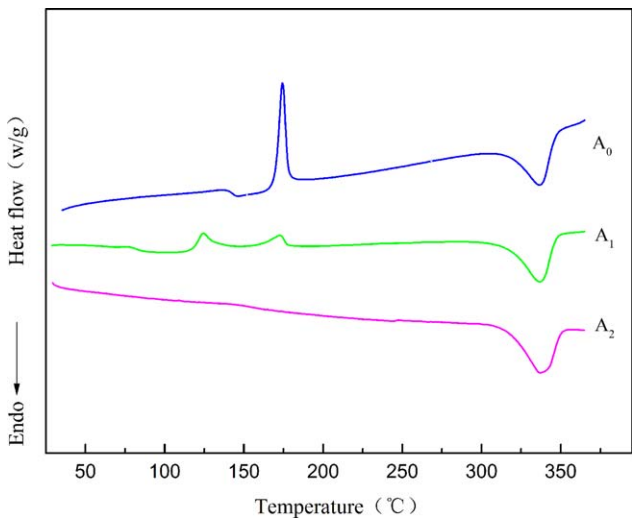


**Figure 4.** DSC thermograms of sample A in different stages of the solid-state foaming process. [Color figure can be viewed in the online issue, which is available at wileyonlinelibrary.com.]

**Table IV.** Characteristic Temperatures, Enthalpy Values, and Crystallinities Calculated from DSC Thermograms

| Sample | $T_g$ (°C) | $T_{cc}$ (°C) | $T_m$ (°C) | $\Delta H_{cc}$ (J/g) | $\Delta H_m$ (J/g) | $X_c$ (%) |
|---|---|---|---|---|---|---|
| $A_0$ | 141 | 176 | 339 | 20.3 | 33.2 | 10.0 |
| $A_1$ | 84 | 125/173 | 337 | 7.6/4.9 | 34.8 | 17.1 |
| $A_2$ | 154 | — | 337 | — | 32.1 | 24.7 |

Water uptake was not detected as foamed PEEK samples have a closed-cell structure.

The tensile tests were performed according to ASTM D638 and Type IV sample specifications, using a universal testing machine (SANS CMT5105) at a constant rate of 5 mm/min. The dielectric tests were conducted by an AS2853A dielectric property testing instrument at a frequency of 10 MHz.

## RESULTS AND DISCUSSION

### Gas Saturation and Desorption

In this research, the sorption and desorption behaviors of $CO_2$ in sample A and sample B were investigated in detail. The dependence of $CO_2$ concentration on saturation pressure is shown in Figure 1. It can be seen that sample A has a larger sorption capacity with respect to sample B at all experiment

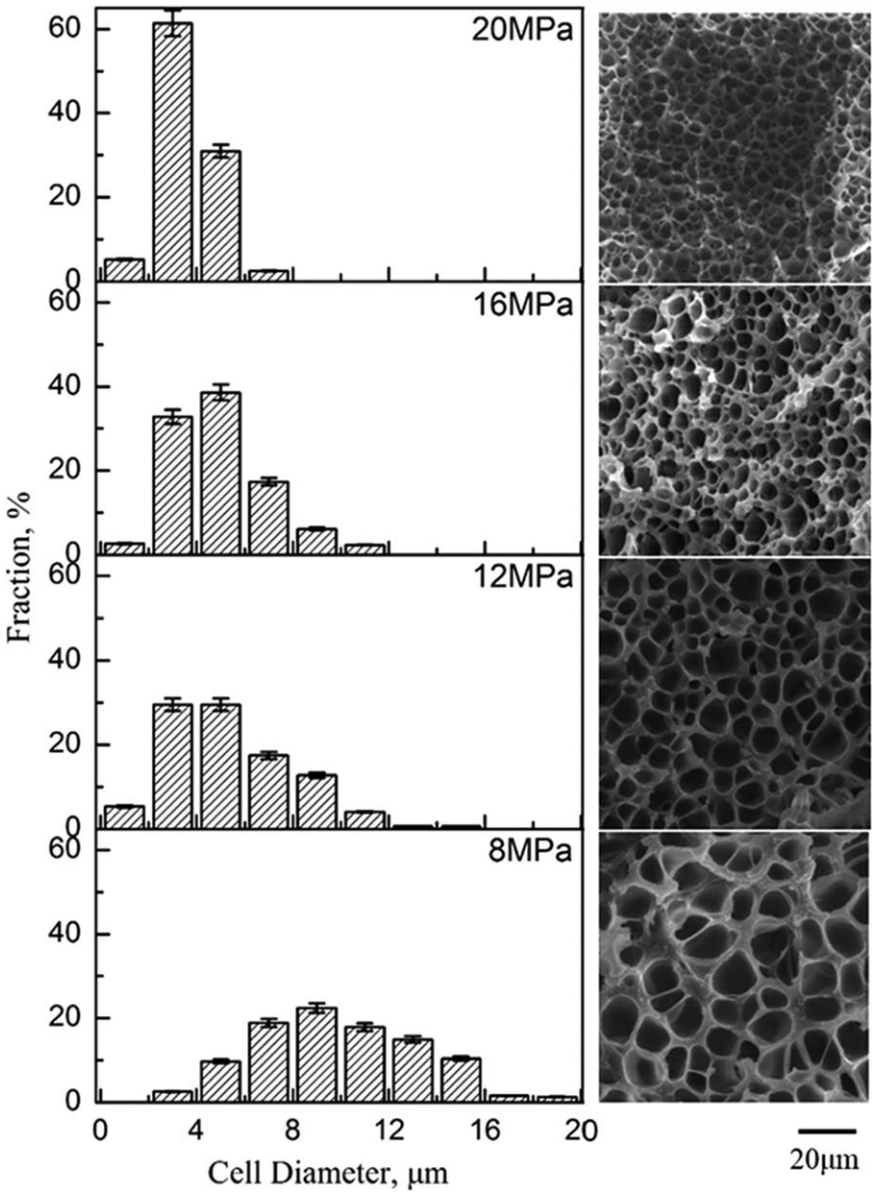


**Figure 5.** Distributions of cell diameter and morphologies of foamed samples prepared under different saturation pressures (samples were saturated at 8, 12, 12, and 20 MPa and 45°C for an adequate time of 9 h, and then foamed in a hot silicon oil bath of 300°C for 5 s).

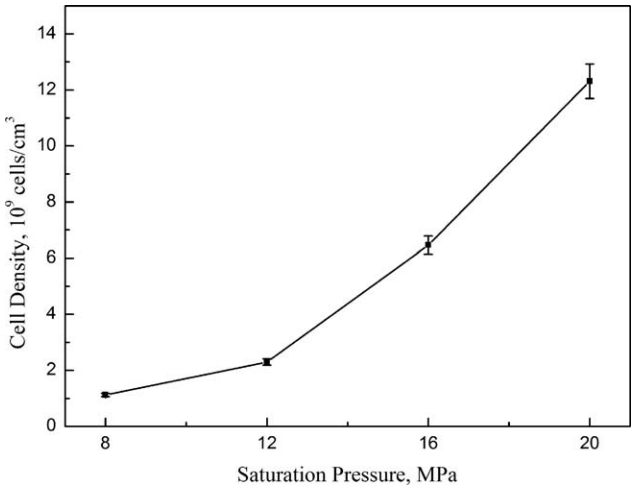


**Figure 6.** Cell density of microcellular PEEK foams as a function of saturation pressure.

pressures. DSC results indicate that sample B presents higher crystallinity than sample A, which was attributed to the different preparation method. The expected reason is that the segment of sample B can form a dense regular crystalline structure, resulting in a scanty free space of polymer matrix to hold $CO_2$. Therefore, sample B presents a poor sorption capacity. It can also be found that $CO_2$ concentration of both PEEK samples increases linearly with the increasing saturation pressure, showing a pressure dependence diffusivity of $CO_2$ in PEEK, which followed the Henry's law:[28–30]

$$C(T_{sat}, P_{sat}) = k_D(T_{sat}) \times P_{sat} \quad (3)$$

Where $C$ is the equilibrium gas concentration, $P_{sat}$ is the saturation pressure, and $k_D$ is the Henry's Law constant. Table II presents the Henry's Law constant of sample A and sample B calculated from adsorption curves of Figure 1. It can be seen that $k_D$ of sample A is larger than sample B, which means that sample B has a poor pressure dependence.

Figure 2 shows the plots of $CO_2$ concentration on saturation time. It is clear that $CO_2$ concentration increases as the saturation time extends at the saturation condition of 12 MPa and 45°C. It is shown that sample A has a more rapid $CO_2$ sorption rate, and needs at least 6 h to reach equilibrium concentration. Nevertheless, more time is needed for sample B to reach equilibrium concentration. For sample B, a slow $CO_2$ sorption rate is still kept after saturated 12 h. This can be explained by the dense regular crystalline structures acting as strong obstacles, which inhibit the diffusion of $CO_2$ into polymer matrix.

Equally important to gas saturation in the solid-state foaming process is desorption of gas when the saturated samples were taken out from the high-pressure vessel. The $CO_2$ desorption was conducted after saturated at 12 MPa and 45°C for an adequate time of 9 h. Gas desorption behavior of thermoplastic polymer sheets has been extensively studied and desorption behavior follows the Fickian diffusion mechanism. The desorption diffusivity at a short desorption time were derived using the following simplified equation:[31]

$$\frac{M_d}{M_\infty} = 1 - \frac{4}{l}\sqrt{\frac{D_d t_d}{\pi}} \quad (4)$$

Where $M_d$ is the $CO_2$ concentration in the samples at time $t_d$ during the desorption process; $M_\infty$ is the $CO_2$ concentration in the samples after saturated for sufficiently long time, and simultaneously the amount of gas at the beginning of desorption; $l$ is the sample thickness; $D_d$ and $t_d$ are the $CO_2$ desorption rate and time, respectively. According to Eq. (4), the curve of $M_d$ versus the square root of $t_d$ should be linear, as shown in Figure 3. $M_\infty$ is obtained by extrapolating $M_d$ to the zero desorption time. $D_d$ is easily estimated from the slope of the curves, and the value of $M_\infty$. $M_\infty$ and $D_d$ of samples A and B are calculated and summarized in Table III. In contrast to sample A, sample B has a slower $CO_2$ desorption rate of $2.25 \times 10^{-12}$ m$^2$/s. This indicates that the dense regular crystal structure restricts the diffusion of $CO_2$ from the polymer matrix during the desorption process.

### The Thermophysical Behavior in the Solid-State Foaming Process

To investigate the thermophysical behavior of PEEK sample A in the solid-state foaming process, DSC measurements of sample A ($A_0$, $A_1$, and $A_2$) during the solid-state foaming process were sequentially conducted (sample A was saturated at 12 MPa and 45°C for 9 h, and then foamed in a hot silicon oil bath of 260°C for 5 s). $A_0$, $A_1$, and $A_2$ represent the stages of untreated, saturated, and foamed, respectively.

Figure 4 shows the DSC thermogram comparison of sample A in different stages of the solid-state foaming process, and the data calculated from the DSC thermograms are listed in Table IV.

It can be seen from Table IV that the glass transition temperature of $A_1$ is 84°C, showing an obvious decrease in contrast with that of the untreated sample (141°C). This indicates that $CO_2$ can play a role of a plasticizer, causing a depression of the glass transition temperature of thermoplastic polymers. The DSC curve of $A_0$ presents one cold crystallization peak at 176°C, while that of $A_1$ shows two cold crystallization peaks. The cold crystallization peak at 125°C is induced by the plasticization effect of dissolved $CO_2$, while the other one at 173°C represents the inherent cold crystallization peak of PEEK. The molecular chains of the saturated sample are easy to move and rearrange as $CO_2$ dissolved in PEEK matrix, resulting in the phenomenon of double cold crystallization peaks. This phenomenon is quite different from other semicrystalline polymers such as PPS, PP, and PET, which only shows a declined inherent cold crystallization peak. The glass transition and cold crystallization peak of sample $A_2$ could not be observed. The expected reason is that it has been crystallized completely after the saturation and foaming processes.

### Influences of Processing Conditions on Cell Morphology and Material Properties

In order to investigate the effects of processing conditions on cell morphology of the microcellular PEEK foams, Sample A was used to conduct a comprehensive solid-state foaming process. Figure 5 shows the distributions of cell diameter and cell

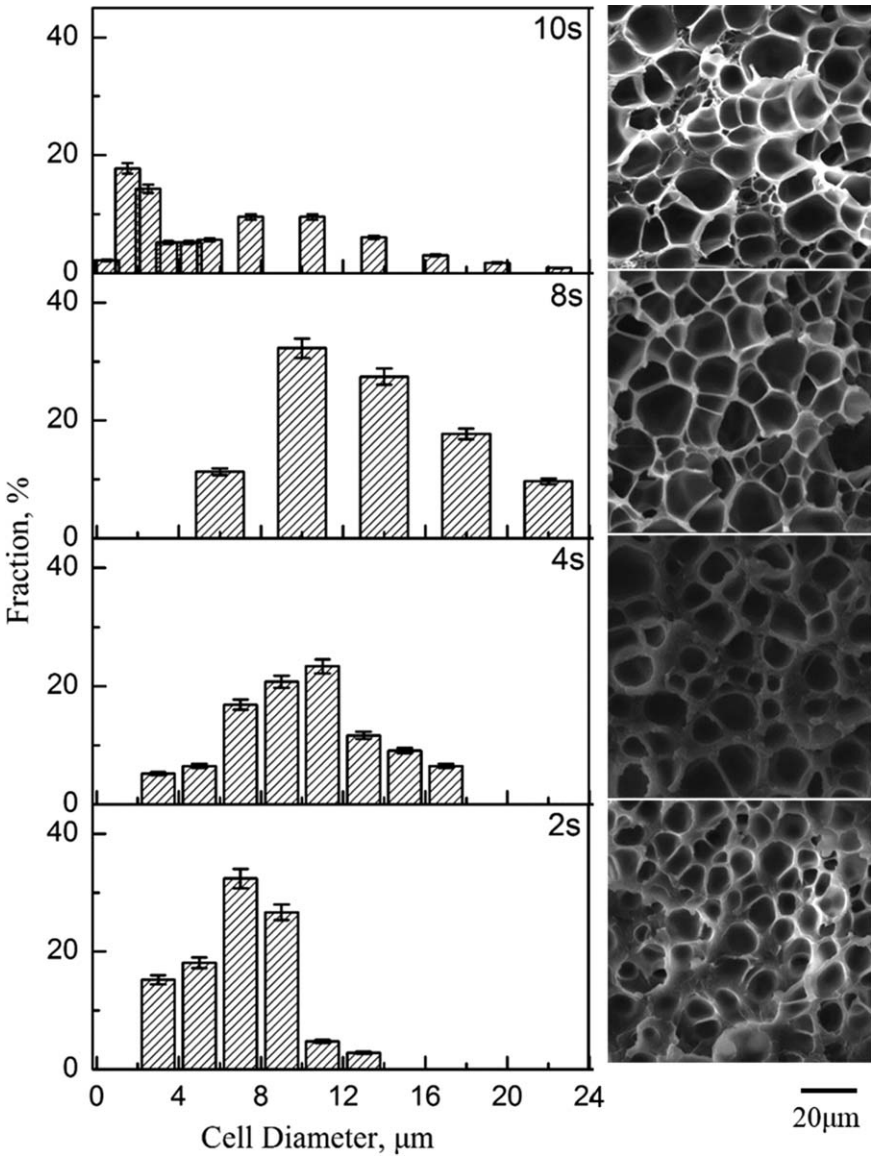


**Figure 7.** Distributions of cell diameter and cell morphologies of microcellular PEEK foams prepared under different foaming times (samples were all saturated at 12 MPa and 45°C for 9 h, and then foamed at 320°C for 2, 4, 6, 8, and 10 s).

morphologies of foamed samples prepared under different saturation pressures. The cell diameters were measured and counted from the corresponding SEM micrographs. It can be seen that the PEEK sample that saturated at a low pressure of 8 MPa has a wide cell diameter distribution range from 2 to 20 $\mu$m. With the increase of saturation pressure, sorption of $CO_2$ on PEEK samples increases. Furthermore, a higher saturation pressure leads to a larger degree of pressure drop during the subsequent rapid depressurization, generating more nucleated cells in the foamed sample. This results in an increase of cell density after foaming. It can be found that the cell size tends to be smaller as the cell nucleation density increases. From Figure 6, it can be seen that the cell density of the microcellular foams prepared under 20 MPa is $1.23 \times 10^{10}$ cells/cm$^3$, which is almost 10 times compared to that under 8 MPa.

To investigate the effect of foaming time on the microcellular foaming of PEEK, the samples were all saturated at 12 MPa and 45°C for 9 h, and then foamed at 320°C for different time. As shown in Figure 7, it is noticed that the microcellular PEEK foam foamed for 2 s has a cell morphology of dispersed spherical structure. With the foaming time extending, the cells expands gradually, and cells with large polyhedral structure were generated when the foaming time is 8 s. With further extending of foaming time, a hierarchical structure with a bimodal cell-size distribution was observed. Compared with SEM micrograph of PEEK sample foamed for 8 s, it can be found that there are plenty of cells with cell diameter smaller than 1 $\mu$m in the matrix between some large cells with a cell diameter of about 10 $\mu$m. From Figure 8, it can be seen that cell density decreases as the foaming time extends. However, cell density is increased when foamed for a foaming time of 10 s.

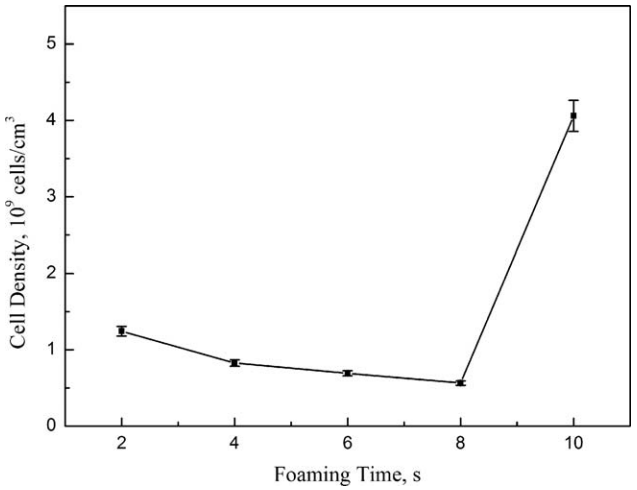


**Figure 8.** Cell density of microcellular PEEK foams prepared under different foaming time.

This phenomenon could be explained by the fact that the temperature of the sample rises from 25 to 320°C quickly when the sample is placed in the silicon oil bath at 320°C. Since most of the molecular chains of sample A were in the amorphous state, the frozen molecular chain segments have a trend to complete the crystallization at a temperature higher than its $T_{cc}$. It is easy to understand that the gas expansion process and the crystallization process occur in company with the molecular chain movement in the foaming process, and some large cells with a diameter of about 10 $\mu$m are first formed in the amorphous regions. When the foaming temperature reached 320°C, the new formed crystalline regions begin to melt with the foaming time extending (the DSC thermogram in Figure 4 shows that Sample A begins to melt at a temperature of about 320°C). This may generate a large amount of heterogeneous nucleated cell sites in the melting newly formed crystalline regions. Finally, dense small cells with a diameter of tens to hundreds of nanometers generate in the matrix among the formed large cells. The comparison of SEM micrographs also reveals the fact that a certain foaming time is needed for the completely foaming of PEEK sheets.

The effect of foaming temperature on the solid-state foaming behavior was investigated, and the obtained results are shown in Figures 9 and 10. It can be seen that numerous spherical cells with a small cell size and a narrower cell-size distribution are dispersed in the PEEK sample foamed at 240°C. With the foaming temperature elevating, the cell size increases gradually. Polyhedral cell structures are generated when the foaming temperature is 320°C. Furthermore, the cell-size distribution becomes wider and the cell density decreases with the foaming temperature range from 240 to 320°C. This phenomenon can be explained by the principle that an elevated foaming temperature reduces the matrix viscosity and makes the easier diffusion of $CO_2$, resulting in a larger cell size. The results imply that the cell morphology could be controlled through sequentially altering foaming time or foaming temperature. With further increasing of the foaming temperature, a bimodal cell-size distribution is observed at the foaming temperature of 340°C. This can be explained by the fact that a higher foaming temperature makes it easier for large cells forming in amorphous regions, as well as dense small cells generating in the melting new-formed crystalline region.

Importantly, it is found from Figures 7 and 9 that a bimodal cell-size distribution is obtained after foaming at 340°C for at least 5 s, while it needs a longer foaming time of at least 10 s when foamed at 320°C. However, it is not observed when foaming at 300°C even for a sufficient foaming time of 60 s. This implies that a less time is needed for the formation of the bimodal cell morphology at a higher temperature. But the bimodal distribution cell morphology cannot be formed when the foaming temperature is below a critical threshold of 320°C.

Several properties of sample A are measured, and the results are listed in Table V. Compared with the unfoamed PEEK sample, the foamed PEEK samples have a continuous decrease in the mass density of sample A with the increase of foaming temperature or foaming time. The porosity of the foamed PEEK samples shows an upward trend, while the dielectric constant shows a downward trend. This may be attributed to the introduction of gas, which has a low dielectric constant of about 1.0. Tensile strength of samples decreases sequentially as foaming temperature increasing or foaming time extends. Specific strength is obtained by the ratio of strength and mass density. It is clear from Table V that specific strength also shows a decreasing trend, but the foamed samples presents a larger specific strength compared with untreated samples.

**Effect of Thermal History on Foaming Behavior**

To investigate the effect of thermal history on cell morphology of microcellular PEEK foam, PEEK samples with different thermal treatments were prepared. Samples A and B were obtained though quenching in the water and free-cooling in the air after the melt extrusion at 380°C, respectively. After the treatment at 360°C 20 min in an oven, samples A and B was processed by free-cooling and quenching, respectively, named samples A′ and B′. Then DSC tests were conducted on four PEEK samples with different thermal treatments. DSC curves of the samples with different thermal treatments are shown in Figure 11 and the characteristic values are listed in Table I. It can be observed that DSC curves of samples A′ and B′ show multiple melting peaks compared with samples A and B, which indicates that the thermal treatment presents a great influence on the crystallization behaviors of semicrystalline polymers. Samples A and B′ present obvious glass transition and cold crystallization, indicating that samples prepared by quenching in the water display a lower crystallinity.

DSC results show that sample A has low crystallinity, which may be because there exists a large amorphous region and a small imperfect crystalline region. The glass transition and cold crystallization peak of sample B are not obvious, attributed to the high crystalline content of sample B.

After a recrystallization process, some new crystalline structures will be generated at the surface of the pre-existed imperfect crystals as heterogeneous nucleation sites.[17] Therefore, sample

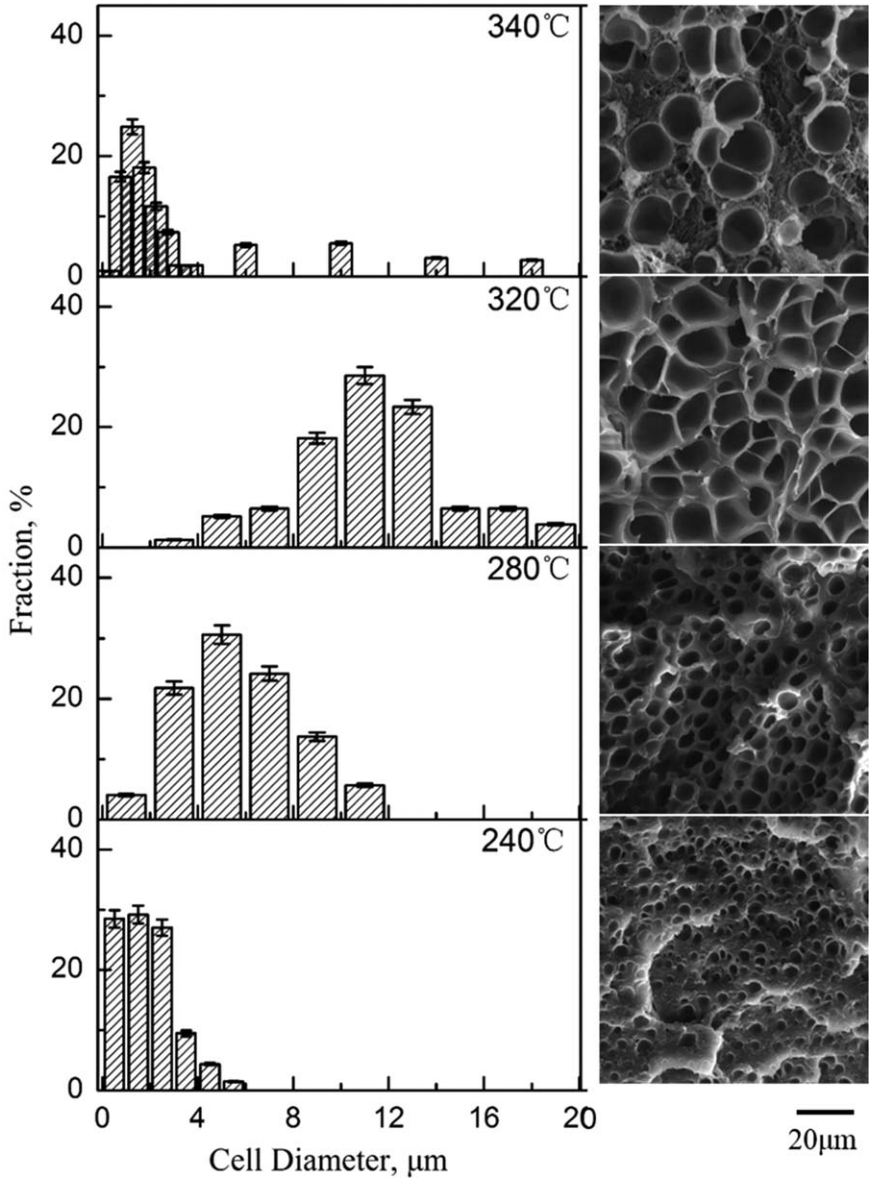


**Figure 9.** Distributions of cell diameter and cell morphologies of microcellular PEEK foams prepared under different foaming temperatures (samples were all saturated at 12 MPa and 45°C for 9 h, and then foamed at 240, 280, 320, and 340°C for 5 s).

A′ also has a high crystalline content. However, The crystallinity of sample A′ is lower than sample B. This could be explained by the fact that only did few imperfect crystals exist in sample. But the new formed crystalline content is less than sample B after the recrystallization process.

The crystals of sample B could be melted during the melting process. Therefore, sample B′, quenched from melting sample B, contains a large amount of imperfect crystals, which result in a higher glass transition temperature (145°C) and a lower cold crystallization temperature (169°C) compared to sample A. This may be attributed to the poor segmental mobility of sample B′ with higher crystallinity.

Cell morphologies of foams prepared from samples with different heat treatments are shown in Figure 12. It can be seen that foamed sample A shows a bimodal distribution of cell morphology, while sample A′ has large cells with average cell size of about 30 $\mu$m. For sample B, there exist a few dispersed spherical cells, while sample B′ has a dense cell structure with a cell size less than 0.1 $\mu$m.

The difference in cell morphologies can be explained by the different processes of heat treatment, which may result in differences in crystalline distributions in the PEEK samples. After sample A was quenched in the water, it showed a recrystallization process at $T_{cc}$ on heating. When foamed above the critical temperature of 320°C, a large amount of cells with a diameter of tens to hundreds of nanometer can be generated in the newly formed crystalline region, which exists among the previously formed cells. This results in the observation of the

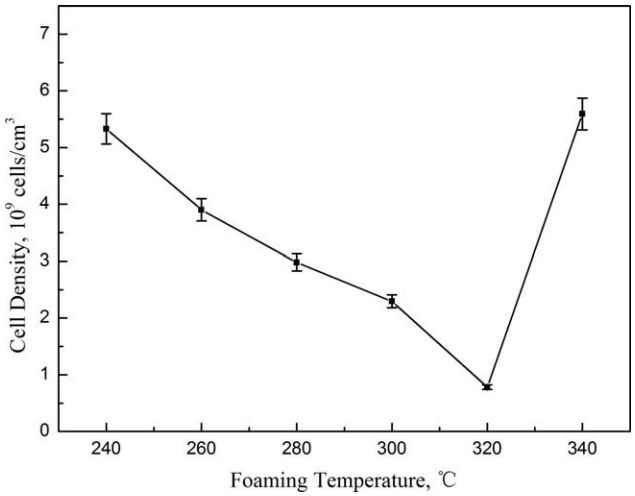


**Figure 10.** Cell density of microcellular PEEK foams prepared under different foaming temperatures.

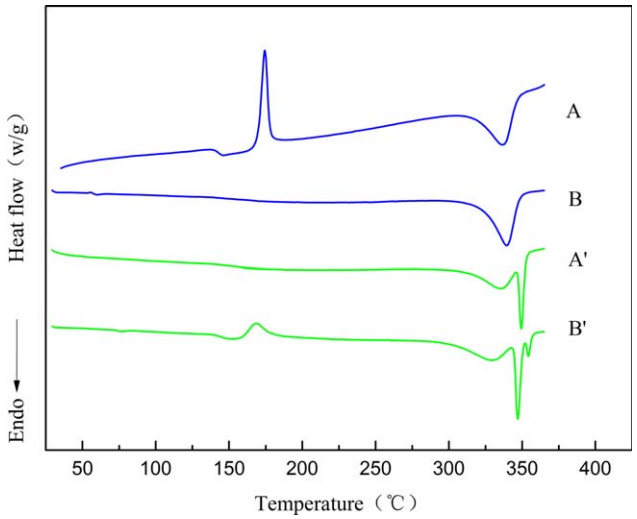


**Figure 11.** DSC thermogram comparison of PEEK samples with four crystallinities. [Color figure can be viewed in the online issue, which is available at wileyonlinelibrary.com.]

bimodal cell-size distribution. For sample B, a few dispersed spherical cells can be generated. This is because the higher crystalline content in the sample B results in less $CO_2$ dissolved in the sample. The crystalline content of sample A′ is less than sample B. The possible reason is that there is no imperfect crystalline region after a recrystallization process. Therefore, only could some large cells be formed in the amorphous region of sample A′. After a melting and then quenching process, sample B′ has a large amount of imperfect crystallization regions, and the recrystallization would occur concurrently with the gas expansion process during the foaming process. The imperfect crystallization regions not only play as numerous heterogeneous nucleated cell sites but also restrict the expansion of cells during the recrystallization process. Therefore, a dense cell structure with cells less than 0.1 $\mu$m was formed.

## CONCLUSION

Microcellular PEEK foams were prepared using the solid-state foaming technique with supercritical $CO_2$ as a physical blowing agent. PEEK with a high crystallinity presents a slower adsorption and desorption rate. The saturated PEEK sample with low crystallinity shows two cold crystallization peaks, including the cold crystallization peak at 125°C induced by the dissolved $CO_2$ and the inherent cold crystallization peak of PEEK at 173°C. The cell density of microcellular PEEK foams increases as the saturation pressure increases. The cell density of the microcellular foams prepared under 20 MPa is 1.23 × $10^{10}$ cells/cm$^3$, which is almost 10 times compares to that under 8 MPa. The cell size increases as the foaming time extends or the foaming temperature increases. It is interesting that the bimodal distribution cell morphology is generated when foamed at temperatures higher than 320°C for a sufficient time. It is found that the crystallization process presents a significant impact on the cell morphology. The sample with a high crystallinity is hardly foamed. However, nanocellular foams with a cell size less than 0.1 $\mu$m can be obtained from a high-crystallized sample after the decrystallization process.

**Table V.** The Property Comparison of Untreated Sample A and Foamed Sample A

| Saturation parameter | Foaming temperature (°C) | Foaming time (s) | Mass density (g/cm$^3$) | Porosity | Dielectric constant | Tensile strength (MPa) | Specific strength (N•m/kg) |
|---|---|---|---|---|---|---|---|
| *Untreated* | | | 1.30 | 0 | 3.11 | 84.97 | 65.25 |
| *12 MPa 45°C 9 h* | *260* | *5* | 0.75 | 0.42 | 2.36 | 61.25 | 81.67 |
| | *280* | | 0.69 | 0.47 | 2.24 | 56.03 | 81.15 |
| | *300* | | 0.66 | 0.49 | 2.06 | 52.24 | 79.60 |
| | *320* | | 0.49 | 0.62 | 1.92 | 35.63 | 73.38 |
| | *340* | | 0.45 | 0.65 | 1.76 | 25.46 | 55.93 |
| | *320* | *2* | 0.65 | 0.50 | 2.04 | 50.11 | 76.83 |
| | | *5* | 0.49 | 0.62 | 1.92 | 35.63 | 73.38 |
| | | *10* | 0.46 | 0.65 | 1.78 | 29.25 | 63.27 |

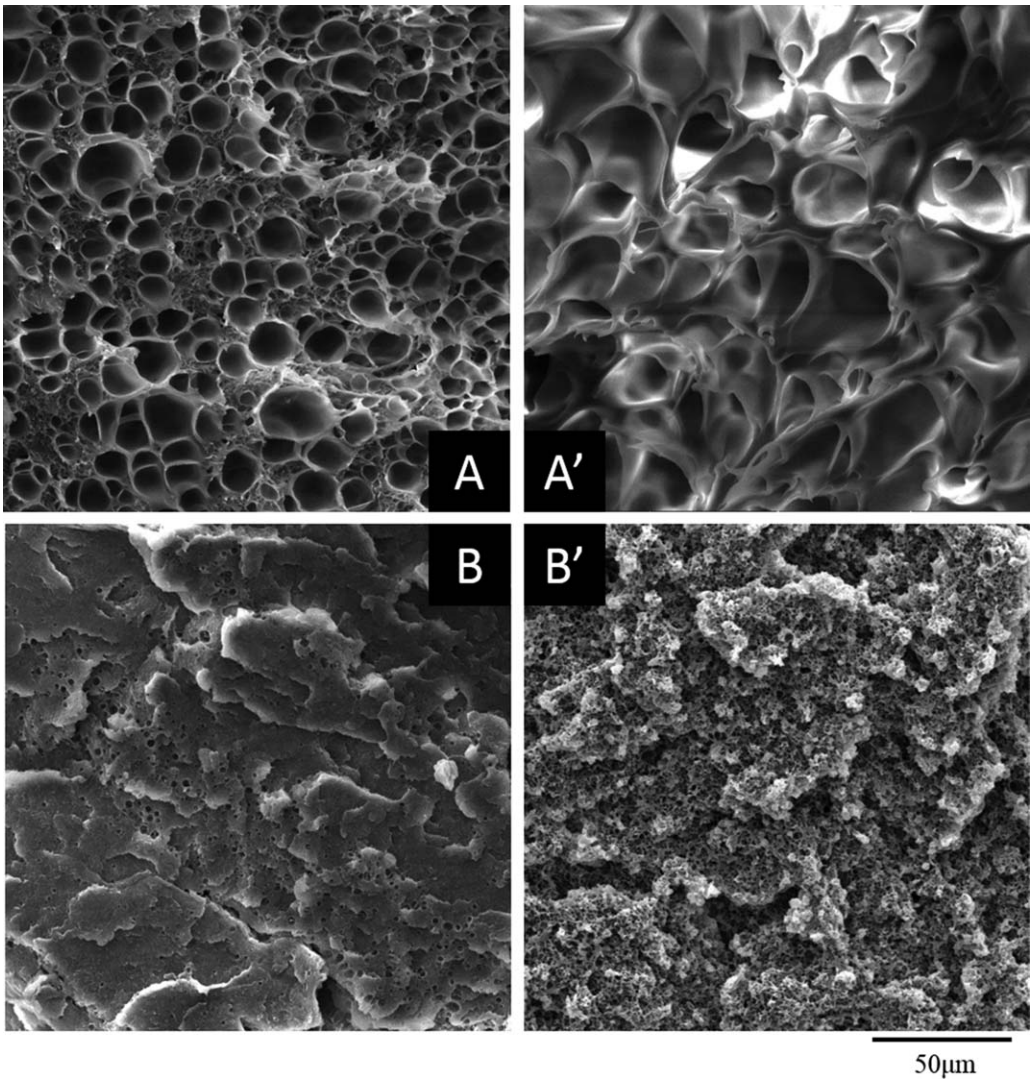


**Figure 12.** Cell morphology of foamed samples with different heat treatments (samples were first saturated at 12 MPa and 45°C for 9 h, and then foamed at 320°C for 10 s).

## REFERENCES


1. Krause, B.; Mettinkhof, R.; Van der Vegt, N. F. A.; Wessling, M. *Macromolecules* **2001**, *34*, 874.
2. Martini, J. E. The Production and Analysis of Microcellular Foam. *Master's Thesis,* MIT: Boston, **1981**.
3. Realinho, V.; Antunes, M.; Martínez, A. B.; Velasco, J. I. *Ind. Eng. Chem. Res.* **2011**, *50*, 13819.
4. Baldwin, D. F.; Park, C. B.; Suh, N. P. *Polym. Eng. Sci.* **1996**, *36*, 1437.
5. Doroudiani, S.; Park, C. B.; Kortschot, M. T. *Polym. Eng. Sci.* **1998**, *38*, 1205.
6. Tsivintzelis, I.; Angelopoulou, A. G.; Panayiotou, C. *Polymer* **2007**, *48*, 5928.
7. Sun, H.; Mark, J. E. *J. Appl. Polym. Sci.* **2002**, *86*, 1692.
8. Abu-Zahra, N. H.; Alian, A. M. *Polym. Plast. Technol. Eng.* **2010**, *49*, 237.
9. Krause, B.; Koops, G. H.; van der Vegt, N. F.; Wessling, M.; Wübbenhorst, M.; van Turnhout, *J. Adv. Mater.* **2002**, *14*, 1041.
10. Matuana, L. M. *Bioresour. Technol.* **2008**, *99*, 3643.
11. Siripurapu, S.; Gay, Y. J.; Royer, J. R.; DeSimone, J. M.; Spontak, R. J.; Khan, S. A. *Polymer* **2002**, *43*, 5511.
12. Mascia, L.; Re, G. D.; Ponti, P. P.; Bologna, S.; Giacomo, G. D.; Haworth, B. *Adv. Polym. Technol.* **2006**, *25*, 225.
13. Ma, Z.; Zhang, G.; Yang, Q.; Shi, X.; Shi, A. *J. Cell. Plast.* **2014**, *50*, 55.
14. Sun, H.; Sur, G. S.; Mark, J. E. *Eur. Polym. J.* **2002**, *38*, 2373.
15. Jin, W.; Xingguo, C.; Mingjun, Y.; Jiasong, H. *Polymer* **2001**, *42*, 8265.
16. Jiang, X. L.; Liu, T.; Xu, Z. M.; Zhao, L.; Hu, G. H.; Yuan, W. K. *J. Supercrit. Fluids* **2009**, *48*, 167.
17. Doroudiani, S.; Park, C. B.; Kortschot, M. T. *Polym. Eng. Sci.* **1996**, *36*, 2645.

18. Itoh, M.; Kabumoto, A. *Furukawa Rev.* **2005**, *28*, 32.
19. Otsuka, T.; Taki, K.; Ohshima, M. *Macromol. Mater. Eng.* **2008**, *293*, 78.
20. Merlet, S.; Marestin, C.; Schiets, F.; Romeyer, O.; Mercier, R. *Macromolecules* **2007**, *40*, 2070.
21. Sun, H.; Mark, J. E.; Tan, S. C.; Venkatasubramanian, N.; Houtz, M. D.; Arnold, F. E.; Lee, C. Y. *Polymer* **2005**, *46*, 6623.
22. Miller, D.; Chatchaisucha, P.; Kumar, V. *Polymer* **2009**, *50*, 5576.
23. Krause, B.; Diekmann, K.; Van der Vegt, N. F. A.; Wessling, M. *Macromolecules* **2002**, *35*, 1738.
24. Xuan, Y.; Gao, Y.; Huang, Y.; Jian, X. *J. Appl. Polym. Sci.* **2001**, *81*, 1487.
25. Shaikh, A. A. G.; Hay, A. S. *J. Polym. Sci., Part A: Polym. Chem.* **2002**, *40*, 496.
26. Hedayati, M.; Salehi, M.; Bagheri, R.; Panjepour, M.; Maghzian, A. *Powder Technol.* **2011**, *207*, 296.
27. King, M. A.; Blundell, D. J.; Howard, J.; Colbourn, E. A.; Kendrick, *J. Mol. Simul.* **1989**, *4*, 3.
28. Kumar, V.; Weller, J. *J. Manuf. Sci. Eng.* **1994**, *116*, 413.
29. Handa, Y. P.; Wong, B.; Zhang, Z.; Kumar, V.; Eddy, S.; Kehmani, K. *Polym. Eng. Sci.* **1999**, *39*, 55.
30. Juntunen, R. P.; Kumar, V.; Weller, J. E.; Bezubic, W. P. *J. Vinyl Addit. Techn.* **2000**, *6*, 93.
31. Wang, D.; Zhao, Y.; Xing, Y.; Gao, H.; Wang, X.; Yang, H. *Polym. Adv. Technol.* **2013**, *24*, 282.